Adaptive DC-Link Voltage-Controlled Hybrid Active Power Filters for Reactive Power Compensation

Chi-Seng Lam, *Student Member, IEEE*, Wai-Hei Choi, *Student Member, IEEE*, Man-Chung Wong, *Senior Member, IEEE*, and Ying-Duo Han, *Senior Member, IEEE*

***Abstract*—This paper presents a novel adaptive dc-link voltage-controlled *LC* coupling hybrid active power filter (*LC*-HAPF) for reducing switching loss and switching noise under reactive power compensation. First, the mathematical relationship between *LC*-HAPF dc-link voltage and reactive power compensation range is deduced and presented. Based on the compensation range analysis, the required minimum dc-link voltage with respect to different loading reactive power is deduced. Then, an adaptive dc-link voltage controller for the three-phase four-wire *LC*-HAPF is proposed, in which the dc-link voltage as well as the reactive power compensation range can be adaptively changed according to different inductive loading situations. Therefore, the compensation range, switching loss, and switching noise of the *LC*-HAPF can be determined and reduced correspondingly. In this paper, the reference dc-link voltage is classified into certain levels for selection in order to alleviate the problem of dc voltage fluctuation caused by its reference frequent variation, and hence reducing the fluctuation impact on the compensation performances. Finally, representative simulation and experimental results of a three-phase four-wire center-split *LC*-HAPF are presented to verify the validity and effectiveness of the proposed adaptive dc-link voltage-controlled *LC*-HAPF in dynamic reactive power compensation.**

***Index Terms*—Active power filters (APFs), dc-link voltage control, hybrid active power filters (HAPFs), passive power filters (PPFs), reactive power control.**

I. Introduction

SINCE the first installation of passive power filters (PPFs) in the mid-1940s, PPFs have been widely used to suppress current harmonics and compensate reactive power in distribution power systems [1] due to their low cost, simplicity, and high-efficiency characteristics. Unfortunately, PPFs have many disadvantages such as low dynamic performance, resonance problems, and filtering characteristics that are easily affected by small variations of the system parameters [2]–[9]. Since the concept of an "active ac power filter" was first developed by L. Gyugyi in 1976 [1], [7], research studies on active power filters (APFs) for current quality compensation are getting more and more attention. APFs can overcome the disadvantages inherent in PPFs, but their initial and operational costs are relatively high [2]–[8] because the dc-link operating voltage should be higher than the system voltage. This slows down their large-scale application in distribution networks. In addition, different hybrid active power filter (HAPF) topologies composed of active and passive components in series and/or parallel have been proposed, aiming to improve the compensation characteristics of PPFs and reduce the voltage and/or current ratings (costs) of the APFs, thus leading to improvements in cost and performance [2]–[16].

The HAPF topologies in [2]–[11] consist of many passive components, such as transformers, capacitors, reactors, and resistors, thus increasing the size and cost of the whole system. A transformerless *LC* coupling HAPF (*LC*-HAPF) has been recently proposed and applied for current quality compensation and damping of harmonic propagation in distribution power systems [12]–[16], in which it has only a few passive components and the dc-link operating voltage can be much lower than the APF. Its low dc-link voltage characteristic is due to the system fundamental voltage dropped across the coupling capacitance but not the active part of the *LC*-HAPF [12]. In addition, the passive part *LC* is designed basing on the fundamental reactive power consumption and the dominant harmonic current of the loading. And the active part is solely responsible for the current harmonics compensation. Therefore, this *LC*-HAPF can only inject a fixed amount of reactive power which is provided by the coupling *LC* and thus achieving a low dc-link voltage level requirement in this special situation. In practical use, the load-side reactive power consumption varies from time to time; the *LC*-HAPF [12]–[16] cannot perform satisfactory dynamic reactive power compensation. The larger the reactive power compensation difference between the load-side and coupling *LC*, the larger the system current and loss, and it will lower the power network stability. In addition, if the loading is dominated by a centralized air-conditioning system, its reactive power consumption will be much higher than the harmonic power consumption [17]. Therefore, it is important and necessary for the *LC*-HAPF to possess dynamic reactive power compensation capability under this loading situation.

Besides, the *LC*-HAPF and other HAPF topologies are all operating at a fixed dc-link voltage level [1]–[16]. Since the switching loss is directly proportional to the dc-link voltage [18],

Manuscript received April 27, 2011; revised July 18, 2011 and September 5, 2011; accepted September 18, 2011. Date of current version February 20, 2012. This work was supported by the Science and Technology Development Fund, Macao SAR Government and Research Committee, University of Macau, Macau, China. Recommended for publication by Associate Editor P.-T. Cheng.

C.-S. Lam, W.-H. Choi, and M.-C. Wong are with the Department of Electrical and Computer Engineering, University of Macau, Macao, China (e-mail: cslam@umac.mo; c.s.lam@ieee.org; hei_choi@ieee.org; mcwong@umac.mo).

Y.-D. Han is with the Department of Electrical Engineering, Tsinghua University, Beijing, China, and also with the Department of Electrical and Computer Engineering, University of Macau, Macao, China (e-mail: ydhan@umac.mo).

Color versions of one or more of the figures in this paper are available online at http://ieeexplore.ieee.org.

Digital Object Identifier 10.1109/TPEL.2011.2169992

the system will obtain a larger switching loss if a higher dc-link voltage is used, and vice versa. Therefore, if the dc-link voltage can be adaptively changed according to different loading reactive power situations, the system can achieve better performances and operational flexibility. Compared with the traditional fixed dc-link voltage *LC*-HAPF, the proposed adaptive dc-link voltage-controlled *LC*-HAPF will experience less switching loss, switching noise, and improve the compensation performances.

In this paper, an adaptive dc-link voltage control scheme for the three-phase four-wire *LC*-HAPF is proposed and studied, so that the switching loss and switching noise can be reduced, and so too the operational cost. However, the maximum compensation range is determined by the specifications of the *LC*-HAPF only, which cannot be affected by this adaptive dc voltage control method. So, it would not affect the initial cost of the *LC*-HAPF either. In order to implement the proposed adaptive control algorithm for *LC*-HAPF, it requires the following.

1) Minimum dc-link voltage with respect to different loading reactive power.
2) Control algorithm for reactive power compensation together with dc-link voltage control.

Unfortunately, due to the limitations in the existing literature, there is no mathematical deduction between the *LC*-HAPF required minimum dc-link voltage and loading reactive power. There are only a few studies investigating the *LC*-HAPF control algorithm for dynamic reactive power compensation together with dc-link voltage control. In the following, a transformerless two-level three-phase four-wire center-split current quality compensator (CCQC) and its single-phase fundamental equivalent circuit model are initially illustrated in Section II. Based on the circuit model, the relationship between the *LC*-HAPF dc-link voltage and reactive power compensation range can be obtained. Then, the required minimum dc-link voltage with respect to different loading reactive power is deduced in Section III. The main contribution of this paper on the adaptive dc-link voltage controller for three-phase four-wire *LC*-HAPF in dynamic reactive power compensation is described in Section IV. The simulation and experimental verification of the proposed adaptive dc-link voltage-controlled *LC*-HAPF is presented in Section V. Given that most of the loads in the distribution power systems are inductive, the following analysis and discussion will only focus on inductive loads [19]. Moreover, as this paper focuses mainly on *LC*-HAPF dynamic reactive power compensation capability analysis, only the *LC*-HAPF reactive power compensation analysis, simulation, and experimental results are included in this paper.

II. Transformerless Two-Level Three-Phase Four-Wire CCQC

A transformerless two-level three-phase four-wire CCQC is shown in Fig. 1, where the subscript "x" denotes phase a, b, c, and n. v_{sx} is the system voltage, v_x is the load voltage, L_s is the system inductance normally neglected due to its low value relatively, thus $v_{sx} \approx v_x$. i_{sx}, i_{Lx}, and i_{cx} are the system, load, and inverter current for each phase. PPF is the coupling

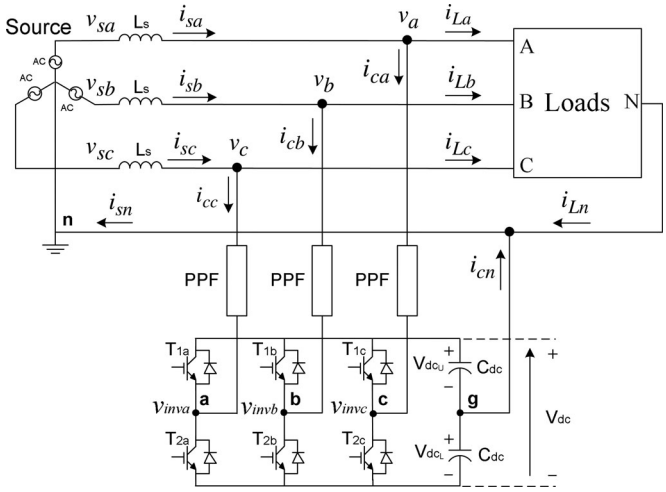

Fig. 1. Configuration of a transformerless two-level three-phase four-wire CCQC.

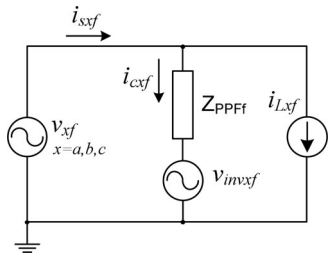

Fig. 2. CCQC single-phase fundamental equivalent circuit model.

passive power filter part, which can be composed of a resistor, inductor, capacitor, or any combinations of them. $C_{\rm dc}$, $V_{{\rm dc}_U}$, and $V_{{\rm dc}_L}$ are the dc capacitance, upper and lower dc capacitor voltages with $V_{{\rm dc}_U} = V_{{\rm dc}_L} = 0.5\,{\rm V_{dc}}$. The dc-link midpoint is assumed to be ground reference g. From Fig. 1, the inverter line-to-ground voltages $v_{{\rm invx}-g}$ will be equal to the inverter line-to-neutral voltages $v_{{\rm invx}-n}$ because the neutral point n is connected to the dc-link midpoint g. Based on the pulsewidth modulation (PWM) technique, $v_{{\rm invx}-n}$ can be simply treated as a controlled voltage source. From the CCQC circuit configuration, as shown in Fig. 1, its single-phase fundamental equivalent circuit model is shown in Fig. 2, where the subscript "f" denotes the fundamental frequency component. In the following analysis, all the parameters are in root-mean-square (rms) values.

For simplicity, v_{sx} and v_x are assumed to be pure sinusoidal without harmonic components (i.e., $\vec{V}_x = \vec{V}_{xf} = |\vec{V}_x| = V_x$). From Fig. 2, the inverter fundamental voltage phasor $\vec{V}_{{\rm invx}_f}$ can be expressed as

$$\vec{V}_{{\rm invx}_f} = \vec{V}_x - \vec{Z}_{{\rm PPF}_f} \cdot \vec{I}_{cx_f}. \tag{1}$$

Here, the fundamental compensating current phasor $\vec{I}_{cx_f}$ of the CCQC can be expressed as $\vec{I}_{cx_f} = I_{cx_{fp}} + jI_{cx_{fq}}$, where the subscripts "$p$" and "$q$" denote the active and reactive components. $I_{cx_{fp}}$ is the fundamental active current for compensating loss and dc-link voltage control, while $I_{cx_{fq}}$ is the fundamental reactive current for compensating reactive power of the loading.

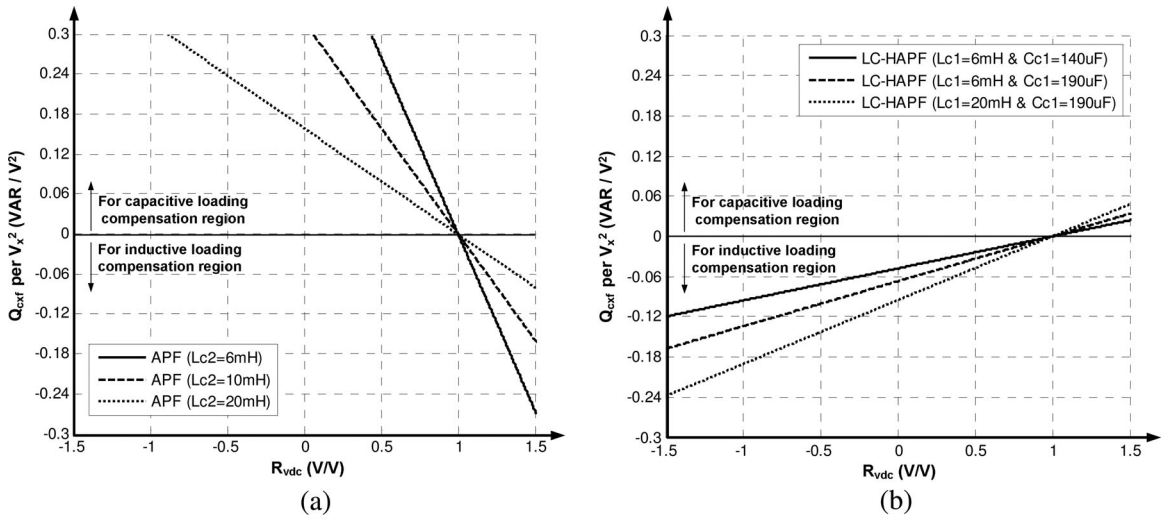

Fig. 3. Q_{cx_f} per V_x^2 with respect to different $R_{V_{\rm dc}}$ for (a) APF and (b) *LC*-HAPF.

Simplify (1) yields

$$\vec{V}_{\text{invx}_f} = V_{\text{invx}_{fp}} + jV_{\text{invx}_{fq}} \tag{2}$$

where

$$\begin{aligned} V_{\text{invx}_{fp}} &= \vec{V}_x + I_{cx_{fq}} X_{\text{PPF}_f} \\ V_{\text{invx}_{fq}} &= -I_{cx_{fp}} X_{\text{PPF}_f}. \end{aligned} \tag{3}$$

From (3), the fundamental compensating active current $I_{cx_{fp}}$ and reactive current $I_{cx_{fq}}$ are

$$I_{cx_{fp}} = -\frac{V_{\text{invx}_{fq}}}{X_{\text{PPF}_f}} \tag{4}$$

$$I_{cx_{fq}} = \frac{V_{\text{invx}_{fp}} - V_x}{X_{\text{PPF}_f}}. \tag{5}$$

Since the CCQC aims to compensate fundamental reactive power, the steady-state active fundamental current $I_{cx_{fp}}$ from the inverter is small ($I_{cx_{fp}} \approx 0$), provided that the dc-link voltage control is implemented. Thus, $V_{\text{invx}_{fq}} \approx 0$. Therefore, the effect of dc-link voltage control for the CCQC system can be simply neglected during steady-state situation.

For a fixed dc-link voltage level $V_{\text{dc}_U} = V_{\text{dc}_L} = 0.5\ \text{V}_{\text{dc}}$ and modulation index m is assumed as $m \approx 1$, $R_{V_{\rm dc}}$ represents the ratio between the dc-link voltage V_{dc_U}, V_{dc_L}, and load voltage V_x reference to neutral n, which can be expressed as

$$R_{V_{\rm dc}} = \frac{\pm V_{\text{invx}f}}{V_x} = \frac{\pm 0.5\,\text{V}_{\text{dc}}/\sqrt{2}}{V_x} = \pm\frac{\text{V}_{\text{dc}}}{2\sqrt{2}\,V_x} \tag{6}$$

where $V_{\text{invx}f}$ is the inverter fundamental rms voltage. If the PPF part is a pure inductor L_{c2}, the CCQC will be the traditional APF. If the PPF part is composed of a series connection of an inductor L_{c1} and a capacitor C_{c1}, the CCQC will be the *LC*-HAPF, in which C_{c1} dominates the passive part at fundamental frequency. With the effect of dc-link voltage control is being neglected ($I_{cx_{fp}} = 0$) at steady state, substituting $X_{\text{PPF}_f} = X_{Lc2_f}$ for APF and $X_{\text{PPF}_f} = -|X_{Cc1_f} - X_{Lc1_f}|$ for *LC*-HAPF, their corresponding fundamental reactive power injection range Q_{cx_f} per square of the load voltage level V_x^2 with respect to different $R_{V_{\rm dc}}$ can be shown in Fig. 3.

Since Q_{cx_f} should be negative for inductive loading compensation, from Fig. 3, the ratio $R_{V_{\rm dc}}$ for APF must be at least greater than 1, while the ratio $R_{V_{\rm dc}}$ for *LC*-HAPF can be smaller than 1 within a specific operational range. This means that the required V_{dc_U}, V_{dc_L} for APF must be larger than the peak of load voltage V_x regardless of the coupling inductance L_{c2}, while the V_{dc_U}, V_{dc_L} for *LC*-HAPF can be smaller than the peak of V_x within that operational range. When $R_{V_{\rm dc}} = 0$, it means that both the APF and *LC*-HAPF are operating at pure passive filter mode, in which the APF at $R_{V_{\rm dc}} = 0$ cannot support inductive loading compensation while the *LC*-HAPF can support a fixed Q_{cx_f}. Moreover, this fixed Q_{cx_f} depends on the passive part parameters. Fig. 3 clearly illustrates the main advantage of *LC*-HAPF over the traditional APF under inductive loading reactive power compensation. Under the same dc-link voltage consideration in Fig. 3(b), when the coupling capacitance C_{c1} or inductance L_{c1} increases, the upper limit of $|Q_{cx_f}|$ for inductive loading compensation region increases; however, the lower limit of $|Q_{cx_f}|$ for that region decreases and vice versa. In the following section, the mathematical deduction details of the *LC*-HAPF fundamental reactive power compensation range with respect to the dc-link voltage under $I_{cx_{fp}} = 0$ assumption will be given. After that, the required minimum dc-link voltage with respect to different loading reactive power can be deduced.

III. *LC*-HAPF Required Minimum DC-Link Voltage With Respect to Loading Reactive Power

Based on the previous assumption that the active fundamental current $I_{cx_{fp}}$ is very small ($I_{cx_{fp}} \approx 0$) at steady state, the inverter injects pure reactive fundamental current $\vec{I}_{cx_f} = jI_{cx_{fq}}$. Therefore, the $\vec{V}_{\text{invx}_f}$ in (2) contains pure active part as $V_{\text{invx}_{fp}} = V_x - I_{cx_{fq}}(X_{Cc1_f} - X_{Lc1_f})$ only. Then, the *LC*-HAPF single-phase fundamental phasor diagram under inductive loading can be shown in Fig. 4. The vertical y-axis can be

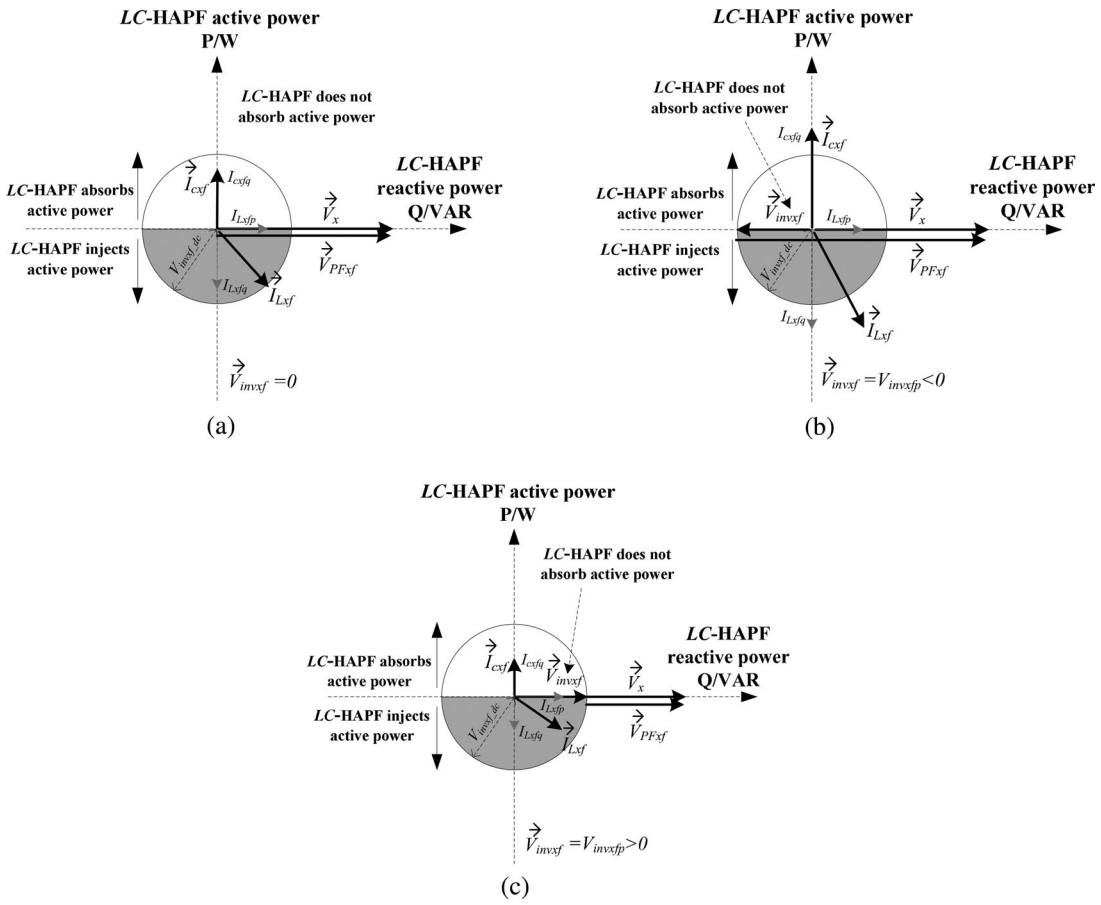

Fig. 4. *LC*-HAPF single-phase fundamental phasor diagram under inductive loading during (a) full-compensation, (b) undercompensation, and (c) overcompensation by passive part.

considered as the *LC*-HAPF active power (P/W) when locating $\vec{V}_x$ onto the *LC*-HAPF horizontal reactive power (Q/VAR) x-axis. The circle and its radius of $V_{\mathrm{invx}_{f\_\mathrm{dc}}} = (0.5\,\mathrm{V_{dc}}/\sqrt{2})$ represent the *LC*-HAPF fundamental compensation range and maximum compensation limit under a fixed dc-link voltage. $\vec{V}_{PFx_f}$ is the fundamental voltage phasor of the passive part. $\vec{I}_{Lx_f}$ is the fundamental load current phasor, where $I_{Lx_{fp}}$ and $I_{Lx_{fq}}$ are the fundamental load active and reactive current. In Fig. 4, the white semi-circle area represents *LC*-HAPF active power absorption region, whereas the shaded semi-circle area represents *LC*-HAPF active power injection region. When $\vec{V}_{\mathrm{invx}_f}$ is located inside the white semi-circle area, the *LC*-HAPF is absorbing active power; on the other hand, the *LC*-HAPF is injecting active power when $\vec{V}_{\mathrm{invx}_f}$ is located inside the shaded semi-circle area. When $\vec{V}_{\mathrm{invx}_f}$ is located onto the Q/VAR x-axis, the *LC*-HAPF does not absorb active power. From Fig. 4, the *LC*-HAPF reactive power compensation range with respect to different dc-link voltage can be deduced.

A. Full-Compensation by Passive Part

When the loading reactive power Q_{Lx_f} is full-compensation by passive part ($Q_{Lx_f} = |Q_{cx_{f\_PF}}|$) as shown in Fig. 4(a), the inverter does not need operation and output voltage ($V_{\mathrm{invx}_{fp}} = 0$). Thus, the switching loss and switching noise will be minimized in this situation. The *LC*-HAPF compensating reactive power Q_{cx_f} is equal to the reactive power provided by the passive part $Q_{cx_{f\_PF}}$, which can be expressed as

$$Q_{cx_f} = Q_{cx_{f\_PF}} = -\frac{V_x^2}{|X_{Cc1_f} - X_{Lc1_f}|} < 0 \qquad (7)$$

where $Q_{cx_{f\_PF}} < 0$ means injecting reactive power or providing leading reactive power.

B. Undercompensation by Passive Part

When the loading reactive power Q_{Lx_f} is undercompensation by passive part ($Q_{Lx_f} > |Q_{cx_{f\_PF}}|$) as shown in Fig. 4(b), in order to generate a larger $I_{cx_{fq}}$, the inverter should output a negative inverter fundamental active voltage ($V_{\mathrm{invx}_{fp}} < 0$), as indicated by (5). With a fixed V_{dc}, the *LC*-HAPF maximum compensating reactive power limit $Q_{cx_{f\_\max}}$ can be deduced through the undercompensation by passive part case, which can be expressed as

$$Q_{cx_{f\_\max}} = -\frac{V_x^2(1+|R_{V_{\mathrm{dc}}}|)}{|X_{Cc1_f} - X_{Lc1_f}|} = Q_{cx_{f\_PF}}(1+|R_{V_{\mathrm{dc}}}|) < 0. \qquad (8)$$

TABLE I
LC-HAPF REACTIVE POWER COMPENSATION RANGE DEDUCTION STEPS UNDER A FIXED DC-LINK VOLTAGE $V_{\mathrm{dc}_U} = V_{\mathrm{dc}_L} = 0.5\ \mathrm{V_{dc}}$

1	With a fixed dc-link voltage $V_{dc_U} = V_{dc_L} = 0.5V_{dc}$: $Q_{cx_{f\_PF}} = -\dfrac{V_x^{\,2}}{\left\lvert X_{Cc1_f} - X_{Lc1_f}\right\rvert} < 0$ (7) $Q_{cx_{f\_max}} = Q_{cx_{f\_PF}}(1+\left\lvert R_{V_{dc}}\right\rvert) < 0$ (8) $Q_{cx_{f\_min}} = Q_{cx_{f\_PF}}(1-\left\lvert R_{V_{dc}}\right\rvert) < 0$ (9) Where $\left\lvert R_{V_{dc}}\right\rvert = \left\lvert \dfrac{V_{dc}}{2\sqrt{2}\,V_x}\right\rvert$ (6)
2	*LC*-HAPF reactive power compensating range for loading Q_{Lx_f}: $\left\lvert Q_{cx_{f\_min}}\right\rvert \le Q_{Lx_f} \le \left\lvert Q_{cx_{f\_max}}\right\rvert$ (10)

C. Overcompensation by Passive Part

When the loading reactive power Q_{Lx_f} is overcompensation by passive part ($Q_{Lx_f} < |Q_{cx_{f\_PF}}|$), as shown in Fig. 4(c), in order to generate a smaller $I_{cx_{fq}}$, the inverter should output a positive inverter fundamental active voltage ($V_{\mathrm{invx}_{fp}} > 0$), as indicated by (5). With a fixed V_{dc}, the *LC*-HAPF minimum compensating reactive power limit $Q_{cx_{f\_\min}}$ can be deduced through the overcompensation by passive part case, which can be expressed as

$$Q_{cx_{f\_\min}} = -\frac{V_x^2(1-|R_{V_{\mathrm{dc}}}|)}{|X_{Cc1_f} - X_{Lc1_f}|} = Q_{cx_{f\_PF}}(1-|R_{V_{\mathrm{dc}}}|) < 0. \tag{9}$$

From (8) and (9), the larger the dc-link voltage V_{dc} or ratio $R_{V_{\mathrm{dc}}}$, the larger the *LC*-HAPF compensation range can be obtained, and vice versa. However, a larger dc-link voltage will increase the *LC*-HAPF switching loss and generate a larger switching noise into the system, while a smaller dc-link will deteriorate the compensating performances if Q_{Lx_f} is outside the *LC*-HAPF compensation range. When V_{dc} is designed, the *LC*-HAPF reactive power compensating range for loading Q_{Lx_f} can be expressed as

$$\left|Q_{cx_{f\_\min}}\right| \le Q_{Lx_f} \le \left|Q_{cx_{f\_\max}}\right|. \tag{10}$$

Table I summarizes the *LC*-HAPF reactive power compensating range deduction steps under a fixed dc-link voltage $V_{\mathrm{dc}_U} = V_{\mathrm{dc}_L} = 0.5\ \mathrm{V_{dc}}$. When Q_{Lx_f} is perfectly compensated by the passive part, the minimum dc-link voltage requirement ($V_{\mathrm{dc}_U} = V_{\mathrm{dc}_L} = 0$) can be achieved. In addition, the larger the reactive power compensation differences between the loading and the passive part, the larger the dc-link voltage requirement and vice versa. From Table I, the required minimum dc-link voltage $V_{\mathrm{dc\_min}\,x}$ in each phase can be found by setting $Q_{Lx_f} \approx |Q_{cx_{f\_\min}}| \approx |Q_{cx_{f\_\max}}|$ in (10)

$$V_{\mathrm{dc\_min}\,x} = 2\sqrt{2}V_x\left|1 - \frac{Q_{Lx_f}}{|Q_{cx_{f\_PF}}|}\right|. \tag{11}$$

Thus, (11) can be applied for the proposed adaptive dc-link voltage control algorithm. Once the Q_{Lx_f} is calculated, the corresponding $V_{\mathrm{dc\_min}\,x}$ in each phase can be obtained. Then, the final three-phase required minimum dc-link voltage $V_{\mathrm{dc\_min}}$ can be chosen as follows:

$$V_{\mathrm{dc\_min}} = \max(V_{\mathrm{dc\_min}\,a}, V_{\mathrm{dc\_min}\,b}, V_{\mathrm{dc\_min}\,c}). \tag{12}$$

In the next section, the adaptive dc-link voltage controller for the three-phase four-wire *LC*-HAPF will be proposed, so that the *LC*-HAPF reactive power compensation range can be determined, and switching loss and switching noise can be reduced compared with the traditional fixed dc-link voltage *LC*-HAPF.

IV. PROPOSED ADAPTIVE DC-LINK VOLTAGE CONTROLLER FOR A THREE-PHASE FOUR-WIRE *LC*-HAPF

Fig. 5 shows the proposed adaptive dc-link voltage control block diagram for the three-phase four-wire *LC*-HAPF, which consists of three main control blocks: instantaneous power compensation control block, the proposed adaptive dc-link voltage control block, and final reference compensating current and PWM control block.

A. Instantaneous Power Compensation Control Block

For the instantaneous power compensation control block, the reference compensating active and reactive currents for *LC*-HAPF (i_{xp}, i_{xq}, the subscript $x = a, b, c$ for three phases) are determined by the three-phase instantaneous pq theory [20].

B. Proposed Adaptive DC-Link Voltage Control Block

The proposed adaptive dc-link voltage control block consists of three parts: 1) determination of adaptive minimum dc-link voltage $V_{\mathrm{dc\_min}}$; 2) determination of final reference dc-link voltage level V_{dc}^*; and 3) dc-link voltage feedback P/PI controller.

1) Determination of Adaptive Minimum DC-Link Voltage: Initially, the loading instantaneous fundamental reactive power

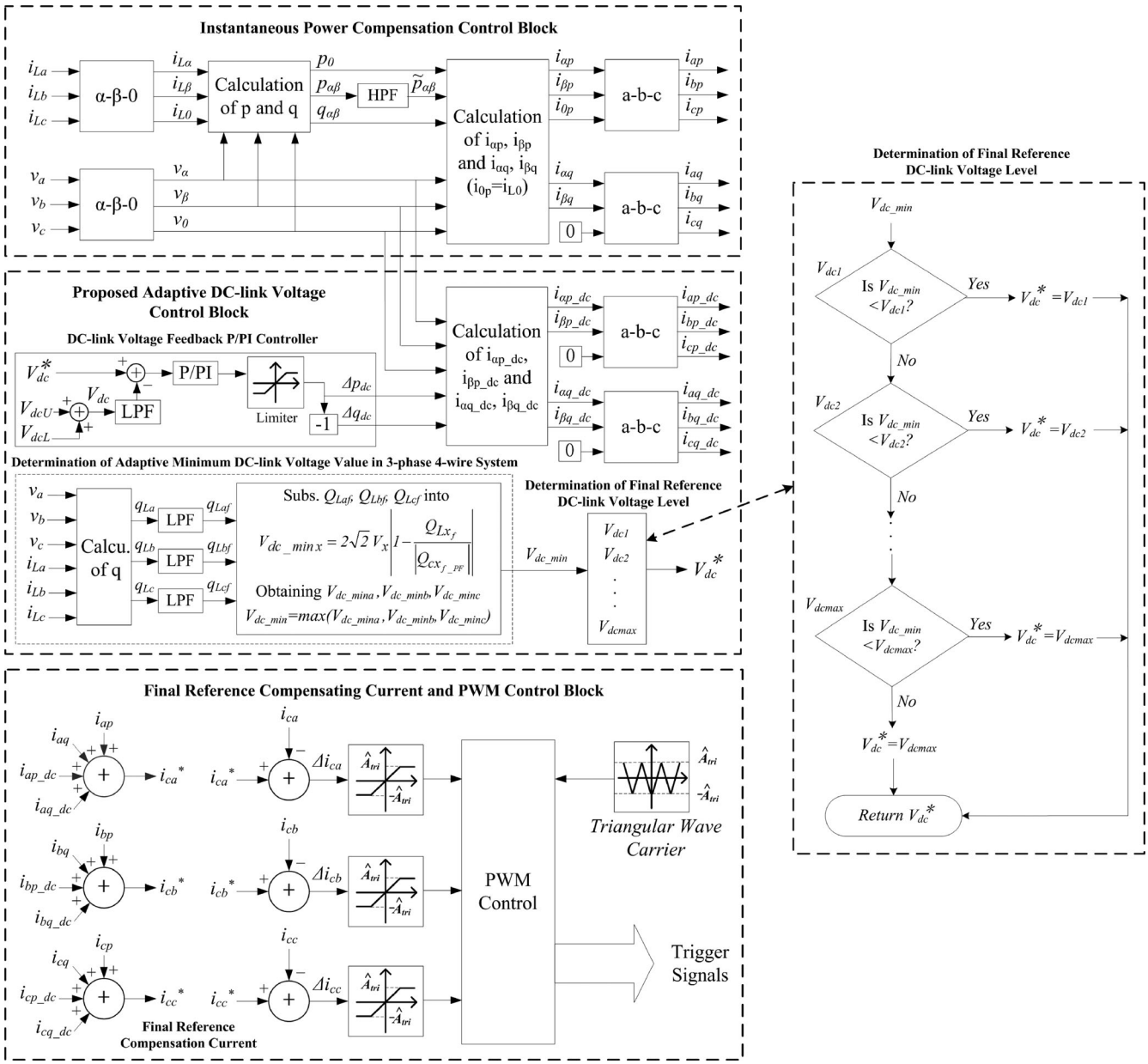

Fig. 5. Proposed adaptive dc-link voltage control block diagram for the three-phase four-wire *LC*-HAPF.

in each phase q_{Lx_f} $(x = a, b, c)$ are calculated using single-phase instantaneous pq theory [21] and low-pass filters. Usually, q_{Lx_f} can keep as a constant value for more than one cycle; thus, Q_{Lx_f} can be approximately treated as $Q_{Lx_f} \approx -q_{Lx_f}$. Then, the required minimum dc-link voltage $V_{\mathrm{dc\_min}\,x}$ for compensating each phase Q_{Lx_f} can be calculated using (11), where V_x is the rms load voltage and $Q_{cx_{f\_PF}}$ can be obtained according to (7). The adaptive minimum dc-link voltage will be equal to $V_{\mathrm{dc\_min}}$, which can be determined by (12). During the balanced loading case, the three-phase fundamental reactive power consumptions are the same ($Q_{La_f} = Q_{Lb_f} = Q_{Lc_f}$), and therefore, $V_{\mathrm{dc\_min}} = V_{\mathrm{dc\_min}\,a} = V_{\mathrm{dc\_min}\,b} = V_{\mathrm{dc\_min}\,c}$. In order to implement the adaptive dc-link voltage control function for the three-phase four-wire LC-HAPF, $V_{\mathrm{dc\_min}}$ can be simply treated as the final reference dc-link voltage V_{dc}^*. It is obvious that when the loading reactive power consumption (Q_{Lx_f}) is changing, the system will adaptively yield different $V_{\mathrm{dc\_min}\,x}$ and $V_{\mathrm{dc\_min}}$ values.

2) Determination of Final Reference DC-Link Voltage Level: However, this adaptive control scheme may frequently change the dc voltage reference V_{dc}^* in practical situations, as the loading is randomly determined by electric users (different Q_{Lx_f}). Then, this frequent change would cause a rapid dc voltage fluctuation, resulting in deterioration of the LC-HAPF operational performances [22]. In order to alleviate this problem, a final reference dc-link voltage level determination process is added as shown in Fig. 5. The final reference dc-link voltage V_{dc}^* is classified into certain levels (V_{dc1}, V_{dc2}, $\ldots$ $V_{\mathrm{dc\,max}}$, $V_{\mathrm{dc1}} < V_{\mathrm{dc2}} \ldots < V_{\mathrm{dc\,max}}$) for selection, so that V_{dc}^* can be maintained as a constant value within a specific compensation

range. From Fig. 5, when the input $V_{\mathrm{dc\_min}}$ is less than the lowest dc voltage level V_{dc1}, the final reference dc-link voltage will be $V_{\mathrm{dc}}^{*} = V_{\mathrm{dc1}}$. If not, repeat the steps until $V_{\mathrm{dc\_min}}$ is found to be less than a dc-link voltage level. However, if $V_{\mathrm{dc\_min}}$ is greater than the maximum voltage level $V_{\mathrm{dc\,max}}$, the final reference dc-link voltage will be $V_{\mathrm{dc}}^{*} = V_{\mathrm{dc\,max}}$. In this way, the dc-link voltage fluctuation problem under the adaptive dc voltage control method can be lessened.

3) DC-Link Voltage Feedback P/PI Controller: In addition, the *LC*-HAPF can effectively control the dc-link voltage by feedback the dc-link voltage error signal as a positive fundamental active and negative fundamental reactive current components ($-\Delta p_{\mathrm{dc}}$, $-\Delta q_{\mathrm{dc}}$). Then, the dc-link voltage V_{dc} can trend its reference V_{dc}^{*} by changing the dc voltage reference compensating currents (i_{xp_dc}, i_{xq_dc}). Therefore, the proposed adaptive dc-link voltage control scheme for the *LC*-HAPF can then be implemented under various inductive linear loading conditions. The adaptive control scheme can apply either P or PI controller for the dc-link voltage control. Even though the P controller can yield a steady-state error, it is chosen because it is simpler and has less operational machine cycles in the digital signal processor (DSP); therefore, it can yield a faster response than the PI controller. If the dc-link voltage with zero steady-state error is taken into consideration, PI controller is appreciated. In addition, the *LC*-HAPF initial start-up dc-link self-charging function can also be carried out by the proposed adaptive dc-link voltage control scheme.

C. Final Reference Compensating Current and PWM Contriol Block

The triangular carrier-based sinusoidal PWM method with current error limiter is applied, so that the compensating current error must be within the triangular wave. And the frequency of the triangular wave is set to $f_{\mathrm{tri}} = 7.5\,\mathrm{kHz}$. After the process of instantaneous power compensation and proposed adaptive dc-link voltage control blocks as in Fig. 5, the final reference compensating current i_{cx}^{*} can be obtained by summing up the i_{xp}, i_{xq}, $i_{\mathrm{xp\_dc}}$, and $i_{\mathrm{xq\_dc}}$. Then, the final reference and actual compensating currents i_{cx}^{*} and i_{cx} will be sent to the PWM control part, and the PWM trigger signals for the switching devices can then be generated. The proposed adaptive dc-link voltage-controlled *LC*-HAPF can compensate the dynamic reactive power and reduce the switching loss and switching noise. In the following, the *LC*-HAPF simulated and experimental compensation results using the proposed adaptive dc-link voltage control algorithm will be given.

V. Simulation and Experimental Verifications of the Proposed Adaptive DC-Link Voltage Controller for the Three-Phase Four-Wire *LC*-HAPF

In this section, the proposed adaptive dc-link voltage-controlled *LC*-HAPF for dynamic reactive power compensation in three-phase four-wire system will be verified by simulations and experiments. Table II lists the simulated and experimental system parameters for the *LC*-HAPF. When the loading reactive power consumption is close to that provided by the passive part at undercompensation and overcompensation situations, the dc-link voltage requirement can be low. In order to show this phenomenon, two sets of passive part parameters for the *LC*-HAPF are chosen for testing. For the undercompensation case, $L_{c1} = 6\,\mathrm{mH}$, $C_{c1} = 140\,\mu\mathrm{F}$, and the passive part supports a fixed reactive power of $Q_{cx_{f\_PF}} = -145.1$ VAR. For the overcompensation case, $L_{c1} = 6\,\mathrm{mH}$, $C_{c1} = 190\,\mu\mathrm{F}$, and the passive part supports a fixed $Q_{cx_{f\_PF}} = -203.5$ VAR. The L_{c1} is designed based on the switching frequency with switching ripple less than 0.5 A under a maximum dc-link voltage of V_{dc_U}, $V_{\mathrm{dc}_L} = 40$ V consideration. Then, the two C_{c1} are designed based on the reactive power consumption for the first inductive loading, and both the first and second inductive loadings listed in Table II.

TABLE II
LC-HAPF System Parameters for Simulations and Experiments

System Parameters		Physical Values
V_x		55 V_{rms}
L_s, R_{c1}		0.5mH, 0Ω
(a) Under-compensation: L_{c1} = 6mH, C_{c1} =140μF $Q_{cx_{f\_PF}} = -145.1\,VAR$	Resistance R_{L1} and inductance L_{L1} for 1st inductive loading	10Ω, 30mH
	Resistance R_{L2} and inductance L_{L2} for 2nd inductive loading	22Ω, 30mH
(b) Over-compensation: L_{c1} = 6mH, C_{c1} =190μF $Q_{cx_{f\_PF}} = -203.5\,VAR$	Resistance R_{L1} and inductance L_{L1} for 1st inductive loading	10Ω, 30mH
	Resistance R_{L2} and inductance L_{L2} for 2nd inductive loading	22Ω, 30mH

In order to simplify the verification in this paper, the simulated and experimental three-phase loadings are approximately balanced as shown in Fig. 6, so that the difference between V_{dc_U} and V_{dc_L} is small ($V_{\mathrm{dc}_U} \approx V_{\mathrm{dc}_L}$) during the adaptive dc-link voltage control. If the three-phase loadings are unbalanced, the dc capacitor voltage imbalance can occur, and the dc capacitor voltage balancing concepts and techniques in [23] and [24] can be applied to balance the V_{dc_U} and V_{dc_L} under the proposed adaptive dc voltage control method.

When the active part is operated together, the *LC*-HAPF can support a reactive power compensation range. As discussed in the previous section, in order to alleviate the dc-link voltage fluctuation problem under the adaptive control method, the final reference dc-link voltage V_{dc}^{*} can be classified into certain levels for selection, in which V_{dc}^{*} is set to have three levels (V_{dc_U}, $V_{\mathrm{dc}_L} = 10$, 20, and 30 V) for the following simulation and experimental verification.

Simulation studies were carried out using PSCAD/EMTDC. In order to verify the simulation results, a two-level three-phase four-wire center-split *LC*-HAPF prototype is also implemented in the laboratory. The control system of the prototype is a DSP TMS320F2407 and the sampling frequency of the *LC*-HAPF system is set at 20 kHz. Fig. 5 shows the *LC*-HAPF control block diagram for both simulations and experiments. Fig. 6 shows the simulated and experimental reactive power at load-side Q_{Lx_f}. When the first inductive loading is connected, the three-phase simulated Q_{Lx_f} are 150.4 VAR with displacement power factor (DPF) $= \cos\theta_{Lxf} = 0.729$, while the three-phase experimental Q_{Lx_f} are 148.5, 146.4, and 145.1 VAR with DPF = 0.763, 0.742, and 0.746, respectively. When both the first and second inductive loadings are connected, the three-phase simulated

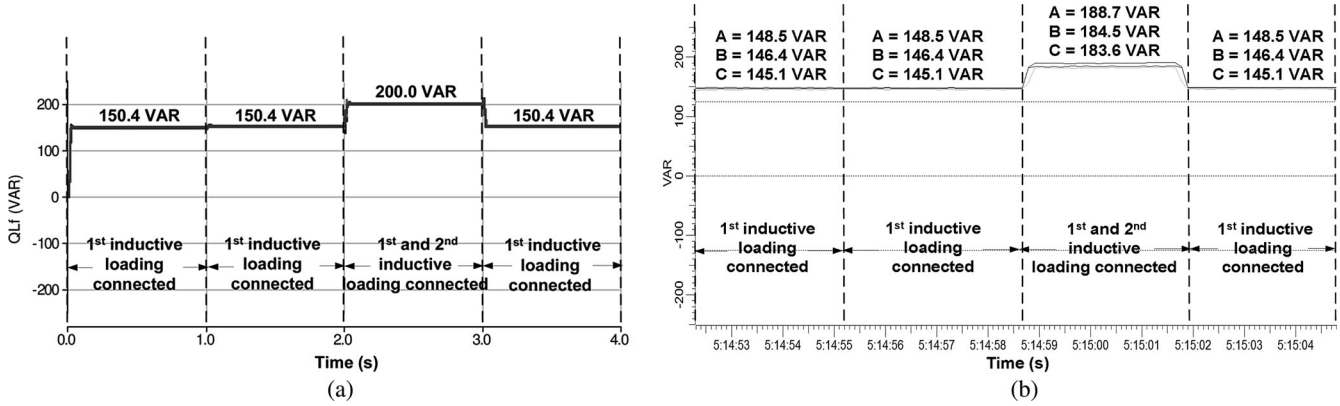

Fig. 6. Q_{Lx_f} for both undercompensation and overcompensation by passive part cases: (a) simulated Q_{Lx_f} and (b) experimental Q_{Lx_f}.

TABLE III
LC-HAPF SIMULATED AND EXPERIMENTAL MINIMUM DC-LINK VOLTAGE LEVEL WITH RESPECT TO Q_{Lx_f} WITHIN V_{dc_U}, V_{dc_L} = 10, 20, AND 30 V

Reactive power by passive part $Q_{cx_{f\_PF}}$	Simulated and experimental Q_{Lx_f} for three phases (VAR)			Required $V_{dc\_min}/2$	Minimum Level V_{dc_U}, V_{dc_L}
(a) Under-compensation: L_{cl}= 6mH, C_{cl}=140μF $Q_{cx_{f\_PF}} = -145.1\,VAR$	1st loading	Sim.	150.4, 150.4, 150.4	2.9V	10V
		Exp.	148.5, 146.4, 145.1	1.8V	10V
	1st & 2nd loadings	Sim.	200.0, 200.0, 200.0	29.5V	30V
		Exp.	188.7, 184.5, 183.6	23.4V	30V
(b) Over-compensation: L_{cl}= 6mH, C_{cl}=190μF $Q_{cx_{f\_PF}} = -203.5\,VAR$	1st loading	Sim.	150.4, 150.4, 150.4	20.3V	30V
		Exp.	148.5, 146.4, 145.1	22.3V	30V
	1st & 2nd loadings	Sim.	200.0, 200.0, 200.0	1.4V	10V
		Exp.	188.7, 184.5, 183.6	7.6V	10V

Q_{Lx_f} increase to 200.0 VAR with DPF = 0.810, while the three-phase experimental Q_{Lx_f} increase to 188.7, 184.5, and 183.6 VAR with DPF = 0.805, 0.815, and 0.822 respectively.

According to the designed three voltage levels (V_{dc_U}, V_{dc_L} = 10, 20, and 30 V) for both simulations and experiments, from Table III, the *LC*-HAPF required minimum dc-link voltage level will be V_{dc_U}, V_{dc_L} = 10 V or V_{dc_U}, V_{dc_L} = 30 V for compensating the first loading or both the first and second loadings during the undercompensation case. During the overcompensation case, the *LC*-HAPF required minimum dc-link voltage level will become V_{dc_U}, V_{dc_L} = 30 V or V_{dc_U}, V_{dc_L} = 10 V for compensating the same loadings. In the following section, the corresponding simulation and experimental results after the proposed adaptive dc-link voltage-controlled *LC*-HAPF compensation will be presented.

A. Undercompensation by Passive Part Situation ($L_{c1} = 6$ mH, $C_{c1} = 140$ μF)

From Table III, the required minimum dc-link voltage level for the *LC*-HAPF is V_{dc_U}, V_{dc_L} = 10 V for the first loading and V_{dc_U}, V_{dc_L} = 30 V for the first and second loadings. Therefore, the proposed adaptive control method for the *LC*-HAPF can reduce the switching loss and switching noise compared with a fixed V_{dc_U}, V_{dc_L} = 30 Vcase. For the simulated and experimental Q_{Lx_f} as shown in Fig. 6, Figs. 7 and 8 illustrate the *LC*-HAPF whole simulated and experimental dynamic process of the adaptive dc-link voltage level and compensation performances during undercompensation by passive part situation. Figs. 7(a) and 8(a) show that the simulated and experimental dc-link voltage level (V_{dc_U}, V_{dc_L}) can be adaptively changed according to different reactive power consumption of the loading. As the simulated and experimental loadings are approximately balanced, only phase b compensation diagrams will be illustrated. From Figs. 7(b) and 8(b), the simulated and experimental system-side reactive power Q_{sx_f} of phase b can be compensated close to zero when the first inductive loading or both the first and second inductive loadings are connected, compared with Fig. 6. Figs. 7(c) and 8(c) show that the simulated and experimental DPF of phase b can be compensated from 0.729 to 1 and 0.742 to 0.999, respectively once the *LC*-HAPF starts operation during the first inductive loading situation. Figs. 7(c) and 8(c) also clearly show that the simulated and experimental system current i_{sx} of phase b can be significantly reduced after the *LC*-HAPF compensation. From Figs. 7(d) and 8(d), the simulated and experimental DPF of phase b can be kept at 0.990 or above when the second loading is connected. The simulation results, as shown in Fig. 7, are consistent with the experimental results as shown in Fig. 8.

Tables IV and V summarize the simulation and experimental compensation results of the proposed adaptive dc-link voltage-controlled *LC*-HAPF during undercompensation by passive part situation. Compared with Q_{Lx_f}, the three-phase simulated Q_{sx_f} (5.0 or 22.0 VAR) and experimental Q_{sx_f} (0.8, −1.5, 3.5

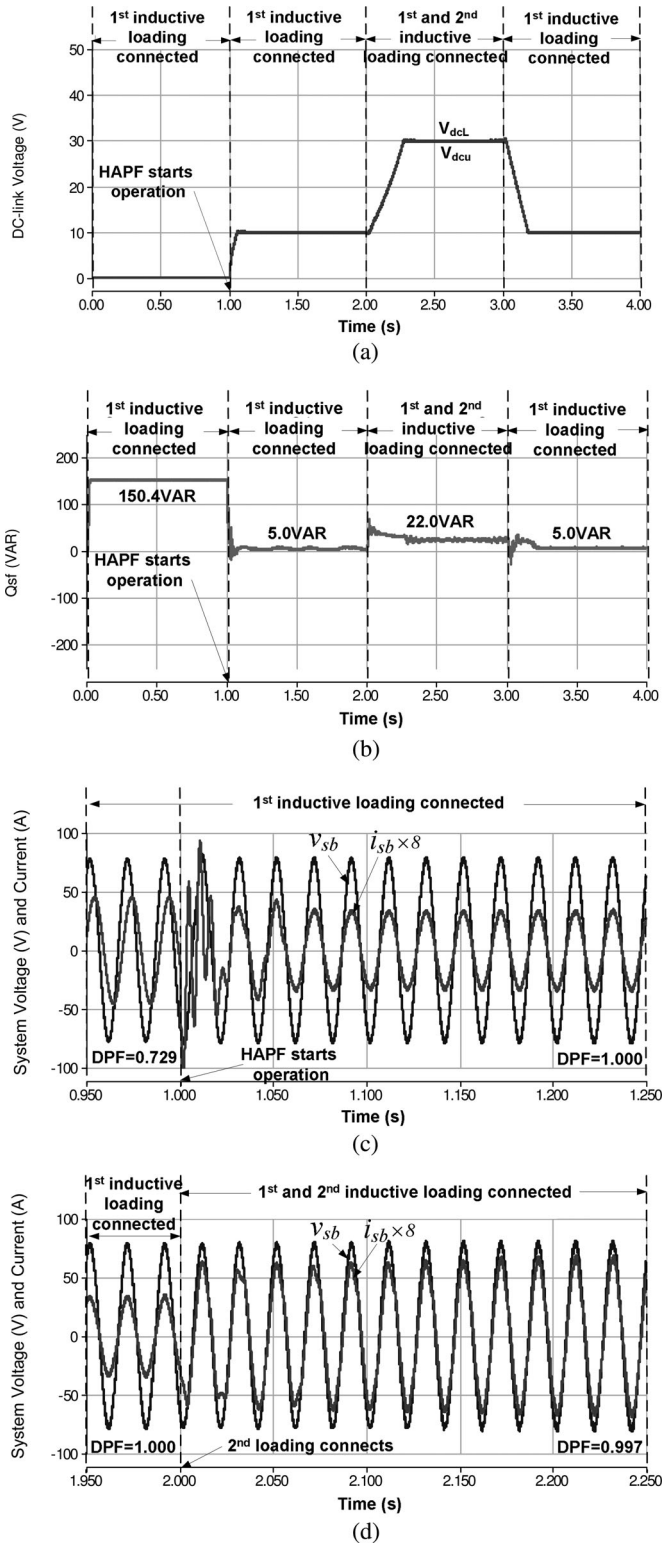

Fig. 7. *LC*-HAPF whole simulated dynamic process during undercompensation by passive part. (a) Adaptive V_{dc_U}, V_{dc_L}. (b) Q_{sx_f} of phase b. (c) DPF of phase b before and after *LC*-HAPF starts operation. (d) DPF of phase b before and after the second loading is connected.

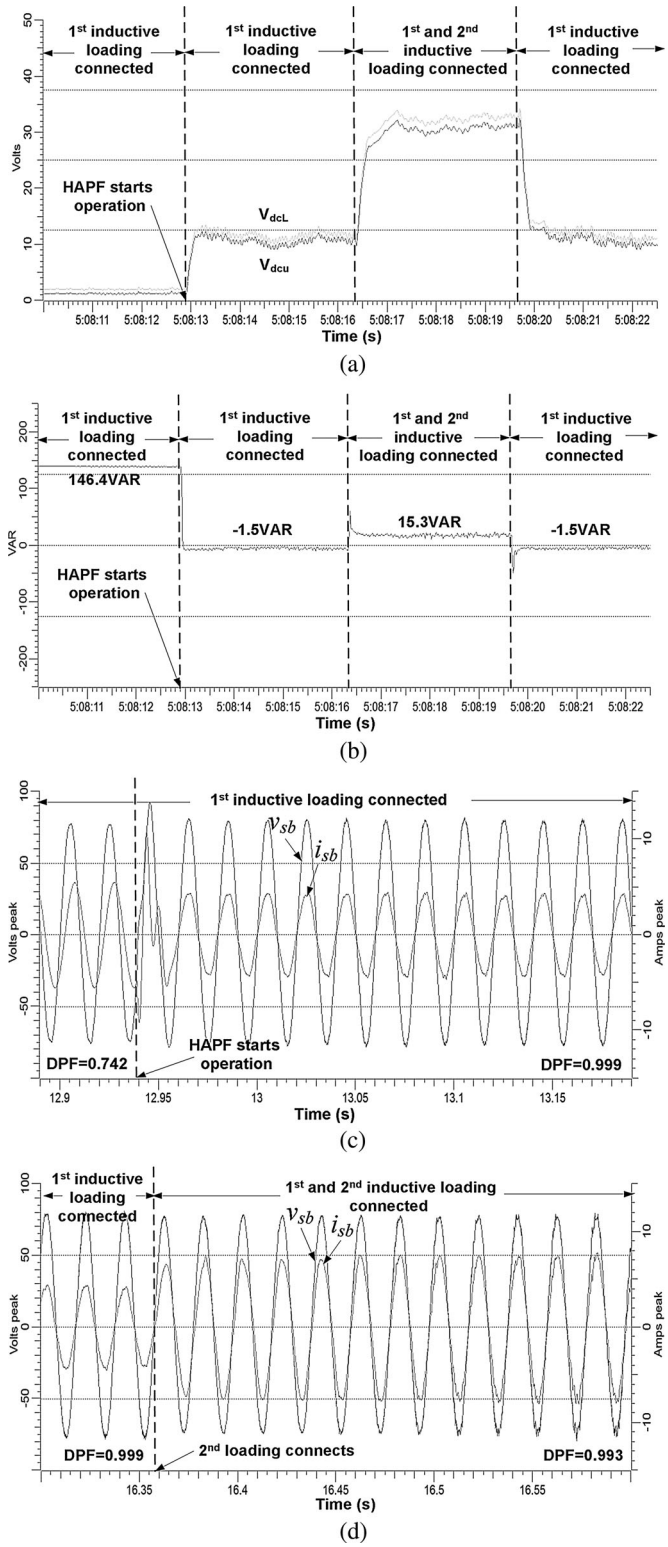

Fig. 8. *LC*-HAPF whole experimental dynamic process during undercompensation by passive part. (a) Adaptive V_{dc_U}, V_{dc_L}. (b) Q_{sx_f} of phase b. (c) DPF of phase b before and after *LC*-HAPF starts operation. (d) DPF of phase b before and after the second loading is connected.

VAR or 25.2, 15.3, 22.2 VAR) have been compensated close to zero when the first loading or both the first and second loadings are connected. These can be verified by showing three-phase simulated and experimental DPF $= 0.990$ or above and $THD_{i_{sx}}$ are within 3.0% and 5.0%, respectively. Moreover, the simulated and experimental i_{sx} can be significantly reduced

TABLE IV
SIMULATION RESULTS BEFORE AND AFTER *LC*-HAPF REACTIVE POWER COMPENSATION WITH AN ADAPTIVE DC-LINK VOLTAGE CONTROL (UNDERCOMPENSATION BY PASSIVE PART, $L_{c1} = 6$ mH, $C_{c1} = 140\ \mu$F)

Different Cases:	Before Compensation				After Compensation			
	Q_{Lx_f} (VAR)	DPF= $cos\,\theta_{Lxf}$	i_{sx} (A_{rms})		Q_{sx_f} (VAR)	DPF= $cos\,\theta_{sxf}$	i_{sx} (A_{rms})	$THD_{i_{sx}}$ (%)
1st inductive loading	150.4	0.729	4.01		5.0	1.000	2.95	2.4
1st and 2nd inductive loading	200.0	0.810	6.25		22.0	0.997	5.04	2.8

TABLE V
EXPERIMENTAL RESULTS BEFORE AND AFTER *LC*-HAPF REACTIVE POWER COMPENSATION WITH AN ADAPTIVE DC-LINK VOLTAGE CONTROL (UNDERCOMPENSATION BY PASSIVE PART, $L_{c1} = 6$ mH, $C_{c1} = 140\ \mu$F)

Different Cases:		Before Compensation			After Compensation			
		Q_{Lx_f} (VAR)	DPF= $cos\,\theta_{Lxf}$	i_{sx} (A_{rms})	Q_{sx_f} (VAR)	DPF= $cos\,\theta_{sxf}$	i_{sx} (A_{rms})	$THD_{i_{sx}}$ (%)
1st inductive loading	A	148.5	0.763	4.06	0.8	0.999	3.04	3.4
	B	146.4	0.742	3.90	-1.5	0.999	3.05	4.9
	C	145.1	0.746	4.01	3.5	0.999	3.02	4.7
1st and 2nd inductive loading	A	188.7	0.805	6.03	25.2	0.990	4.97	3.3
	B	184.5	0.815	5.87	15.3	0.993	4.96	4.1
	C	183.6	0.822	5.94	22.2	0.991	4.90	4.7

after *LC*-HAPF compensation. Figs. 7 and 8 and Tables IV and V verify the proposed adaptive dc-link voltage-controlled *LC*-HAPF for dynamic reactive power compensation during the undercompensation case.

B. Overcompensation by Passive Part Situation ($L_{c1} = 6$ mH, $C_{c1} = 190\ \mu$F)

From Table III, the required minimum dc-link voltage level for the *LC*-HAPF is V_{dc_U}, $V_{\mathrm{dc}_L} = 30$ V for the first loading and V_{dc_U}, $V_{\mathrm{dc}_L} = 10$ V for the first and second loadings. Therefore, the proposed adaptive control method for the *LC*-HAPF can reduce the switching loss and switching noise compared with a fixed V_{dc_U}, $V_{\mathrm{dc}_L} = 30$ Vcase. For the simulated and experimental Q_{Lx_f} as shown in Fig. 6, Figs. 9 and 10 illustrate the *LC*-HAPF whole simulated and experimental dynamic processes of the adaptive dc-link voltage level and compensation performances during overcompensation by passive part situation. Figs. 9(a) and 10(a) show that the simulated and experimental dc-link voltage level (V_{dc_U}, V_{dc_L}) can be adaptively changed according to different reactive power consumption of the loading. From Figs. 9(b) and 10(b), the simulated and experimental Q_{sx_f} of phase b can be compensated close to zero when the first loading or both the first and second loadings are connected. Figs. 9(c) and 10(c) show that the simulated and experimental DPF of phase b can be compensated from 0.729 to 0.998 and 0.742 to 0.989, respectively, once the *LC*-HAPF starts operation. Figs. 9(c) and 10(c) also clearly show that the simulated and experimental system current i_{sx} of phase b can be significantly reduced after the *LC*-HAPF compensation. From Figs. 9(d) and 10(d), the simulated and experimental DPF of phase b can be kept at 0.999 or above when the second loading is connected. The simulation results, as shown in Fig. 9, are consistent with the experimental results shown in Fig. 10.

Tables VI and VII summarize the simulation and experimental compensation results of the proposed adaptive dc-link

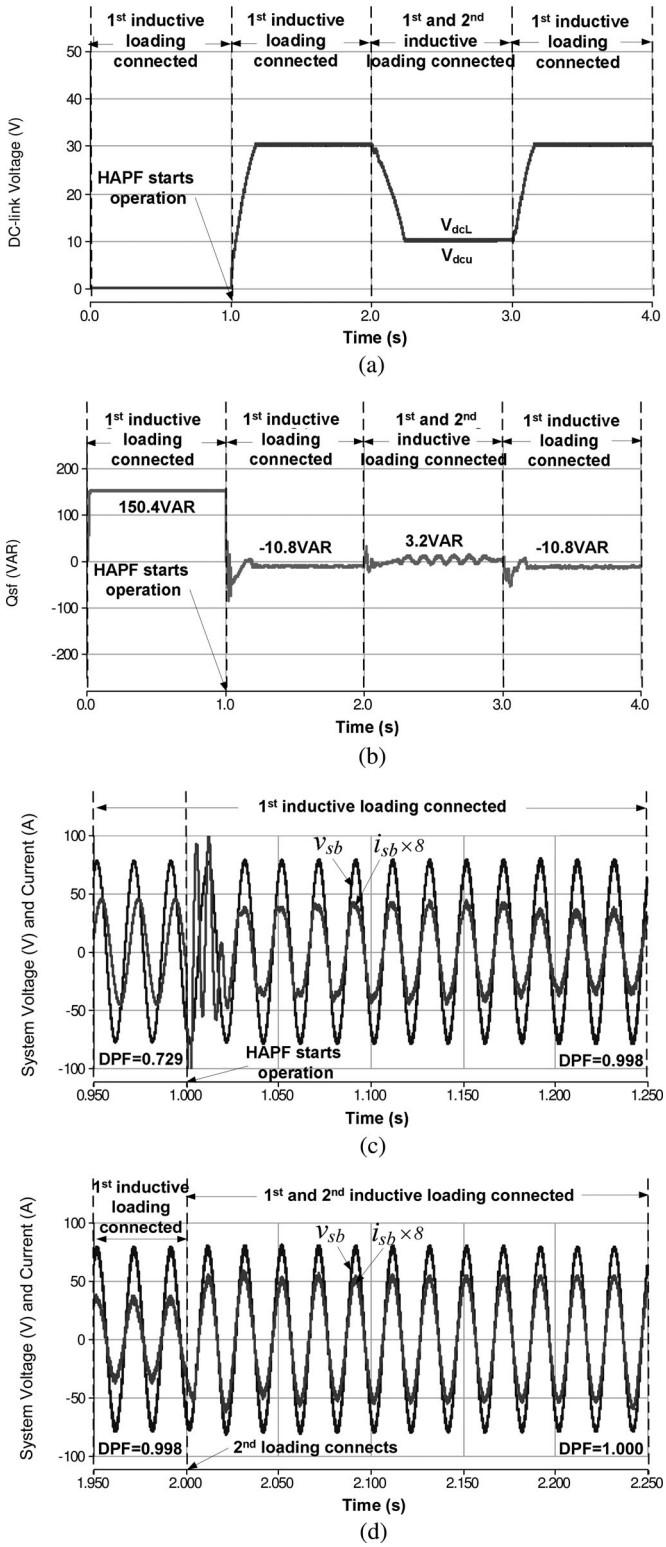

Fig. 9. *LC*-HAPF whole simulated dynamic process during overcompensation by passive part. (a) Adaptive V_{dc_U}, V_{dc_L}. (b) Q_{sx_f} of phase b. (c) DPF of phase b before and after *LC*-HAPF starts operation. (d) DPF of phase b before and after the second loading is connected.

voltage-controlled *LC*-HAPF during overcompensation by passive part situation. Compared with Q_{Lx_f}, the three-phase simulated Q_{sx_f} (-10.8 or 3.2 VAR) and experimental Q_{sx_f} (-13.4,

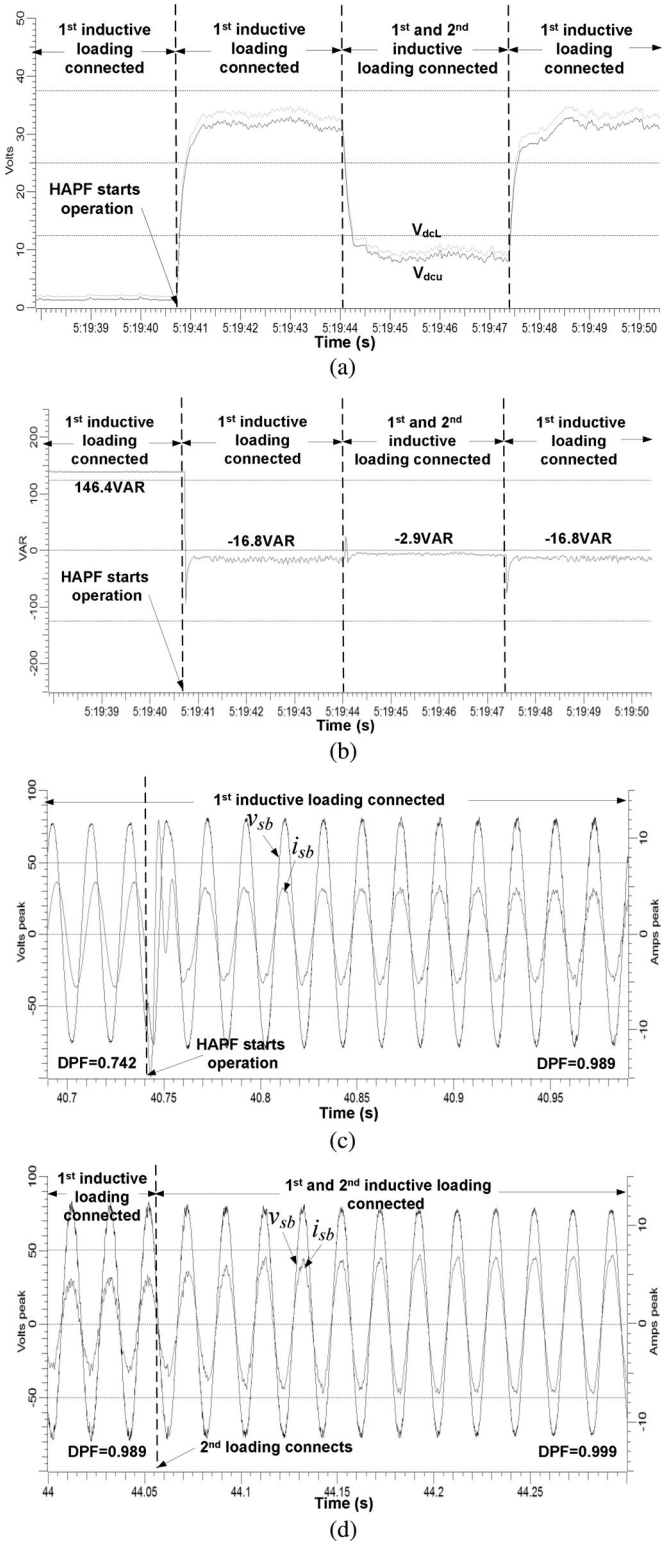

Fig. 10. *LC*-HAPF whole experimental dynamic process during overcompensation by passive part. (a) Adaptive V_{dc_U}, V_{dc_L}. (b) Q_{sx_f} of phase b. (c) DPF of phase b before and after *LC*-HAPF starts operation. (d) DPF of phase b before and after the second loading is connected.

-16.8, -13.8 VAR or -3.4, -2.9, -0.8 VAR) have been compensated close to zero when the first loading or both the first and second loadings are connected. These can be verified by showing

TABLE VI
SIMULATION RESULTS BEFORE AND AFTER *LC*-HAPF REACTIVE POWER COMPENSATION WITH AN ADAPTIVE DC-LINK VOLTAGE CONTROL (OVERCOMPENSATION BY PASSIVE PART, $L_{c1} = 6$ mH, $C_{c1} = 190\ \mu$F)

Different Cases:	Before Compensation			After Compensation			
	Q_{Lx_f} (VAR)	DPF= $cos\,\theta_{Lxf}$	i_{sx} (A_{rms})	Q_{sx_f} (VAR)	DPF= $cos\,\theta_{sxf}$	i_{sx} (A_{rms})	$THD_{i_{sx}}$ (%)
1st inductive loading	150.4	0.729	4.01	-10.8	0.998	2.97	3.7
1st and 2nd inductive loading	200.0	0.810	6.25	3.2	1.000	5.08	3.2

TABLE VII
EXPERIMENTAL RESULTS BEFORE AND AFTER *LC*-HAPF REACTIVE POWER COMPENSATION WITH AN ADAPTIVE DC-LINK VOLTAGE CONTROL (OVERCOMPENSATION BY PASSIVE PART, $L_{c1} = 6$ mH, $C_{c1} = 190\ \mu$F)

Different Cases:		Before Compensation			After Compensation			
		Q_{Lx_f} (VAR)	DPF= $cos\,\theta_{Lxf}$	i_{sx} (A_{rms})	Q_{sx_f} (VAR)	DPF= $cos\,\theta_{sxf}$	i_{sx} (A_{rms})	$THD_{i_{sx}}$ (%)
1st inductive loading	A	148.5	0.763	4.06	-13.4	0.990	3.10	4.3
	B	146.4	0.742	3.90	-16.8	0.989	3.15	5.5
	C	145.1	0.746	4.01	-13.8	0.990	3.03	5.3
1st and 2nd inductive loading	A	188.7	0.805	6.03	-3.4	0.999	5.01	1.9
	B	184.5	0.815	5.87	-2.9	0.999	4.99	2.5
	C	183.6	0.822	5.94	-0.8	0.999	4.91	2.7

three-phase simulated and experimental DPF $= 0.990$ or above and $THD_{i_{sx}}$ are within 4.0% and 6.0%, respectively. Moreover, the simulated and experimental i_{sx} can be significantly reduced after *LC*-HAPF compensation. Figs. 9 and 10 and Tables VI and VII verify the proposed adaptive dc-link voltage-controlled *LC*-HAPF for dynamic reactive power compensation during the overcompensation case.

C. Comparison Between Fixed and Adaptive DC-Link Voltage Control

During undercompensation by passive part case ($L_{c1} = 6$ mH, $C_{c1} = 140\ \mu$F), with a fixed dc-link voltage of V_{dc_U}, $V_{\mathrm{dc}_L} = 30$ V, Figs. 11 and 12 show the *LC*-HAPF whole simulated and experimental dynamic compensation process for the same loading situations as shown in Fig. 6. Comparing Figs. 11 and 12 with Figs. 7 and 8, the fixed and adaptive dc-link voltage control can achieve more or less the same steady-state reactive power compensation results. However, the adaptive control scheme just requires a lower dc-link voltage of V_{dc_U}, $V_{\mathrm{dc}_L} = 10$ V for compensating the first loading as shown in Figs. 7(a) and 8(a). For the adaptive dc-link voltage control of the *LC*-HAPF, due to its final reference dc-link voltage level V_{dc}^* can be varied according to different loading conditions, the compensation performance will be influenced during each changing of the dc voltage level. Compared with the fixed dc-link voltage control, the proposed adaptive control scheme will have a longer settling time during the load and dc voltage level changing situation, which can be verified by the compensated Q_{sx_f} as shown in Figs. 7, 8, 11, and 12.

Figs. 13 and 14 show the *LC*-HAPF simulated and experimental compensating current i_{cx} of phase b and their spectra with 1) a fixed dc-link voltage of V_{dc_U}, $V_{\mathrm{dc}_L} = 30$ V; and 2) the proposed adaptive dc-link voltage control during the first loading connected case. Since the reactive power consumption of the first inductive loading can almost be fully compensated by

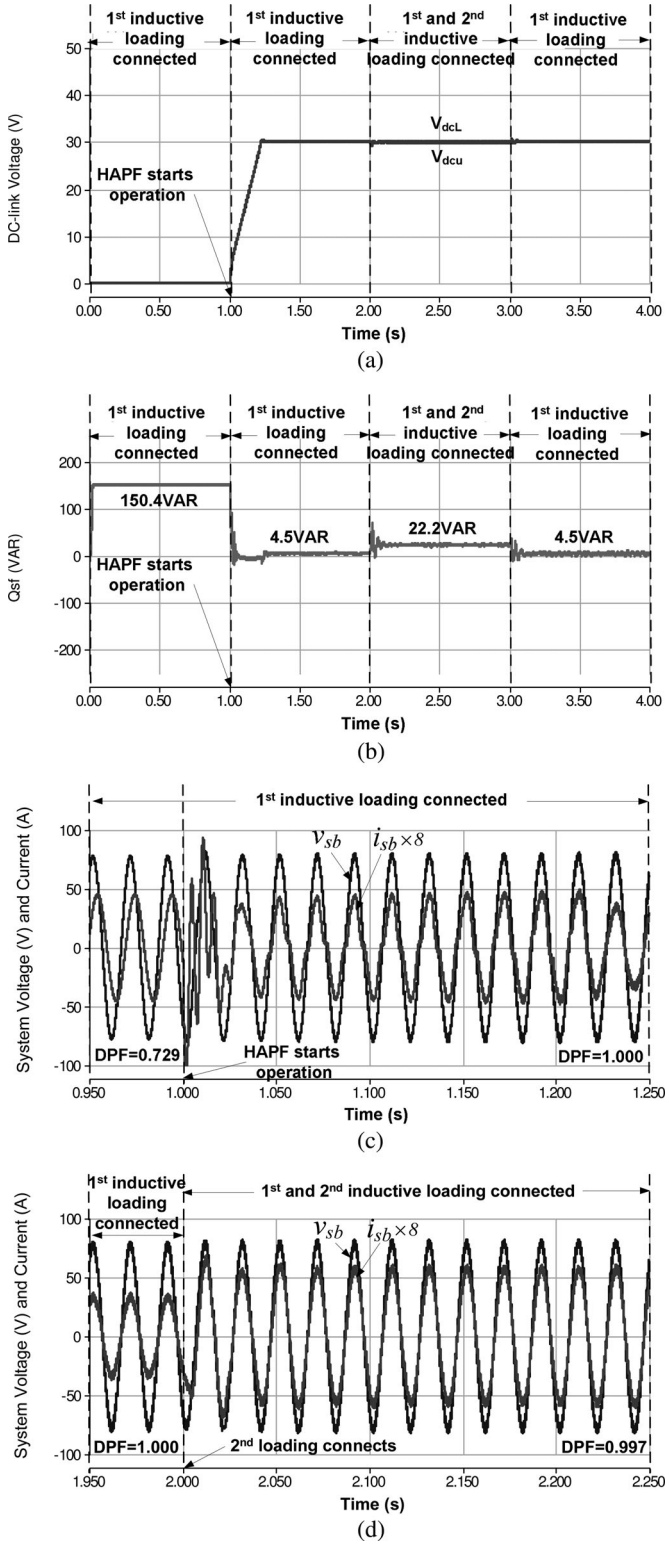

Fig. 11. *LC*-HAPF whole simulated dynamic process during undercompensation by passive part. (a) Fixed V_{dc_U}, $V_{\mathrm{dc}_L} = 30$ V. (b) Q_{sxf} of phase b. (c) DPF of phase b before and after *LC*-HAPF starts operation. (d) DPF of phase b before and after the second loading is connected.

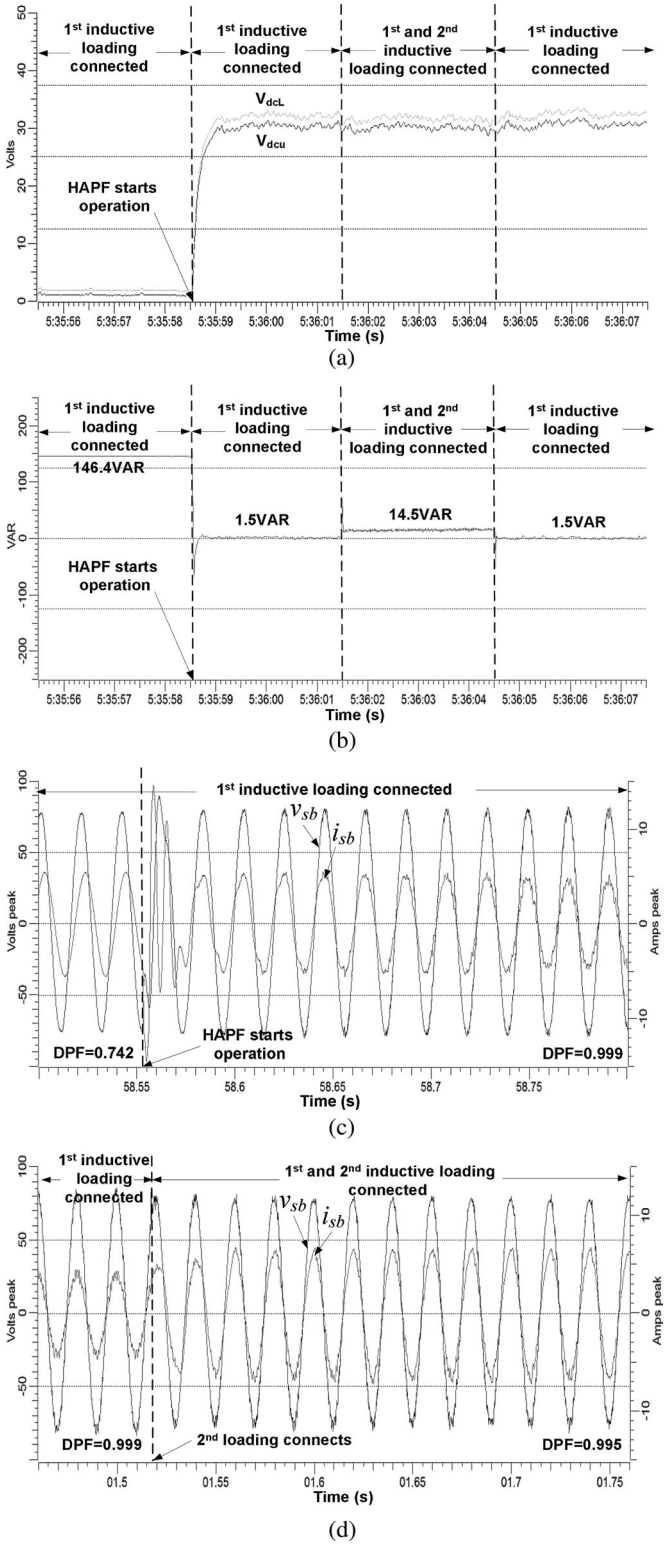

Fig. 12. *LC*-HAPF whole experimental dynamic process during undercompensation by passive part. (a) Fixed V_{dc_U}, $V_{\mathrm{dc}_L} = 30$ V. (b) Q_{sxf} of phase b. (c) DPF of phase b before and after *LC*-HAPF starts operation. (d) DPF of phase b before and after the second loading is connected.

the passive part, as shown in Table III, it is clearly illustrated, in Figs. 13 and 14, that the adaptive dc-link voltage control scheme can effectively reduce the switching noise compared with the traditional fixed V_{dc_U}, $V_{\mathrm{dc}_L} = 30$ V operation. Therefore, the proposed adaptive control method for the *LC*-HAPF can reduce the switching loss and switching noise compared with the

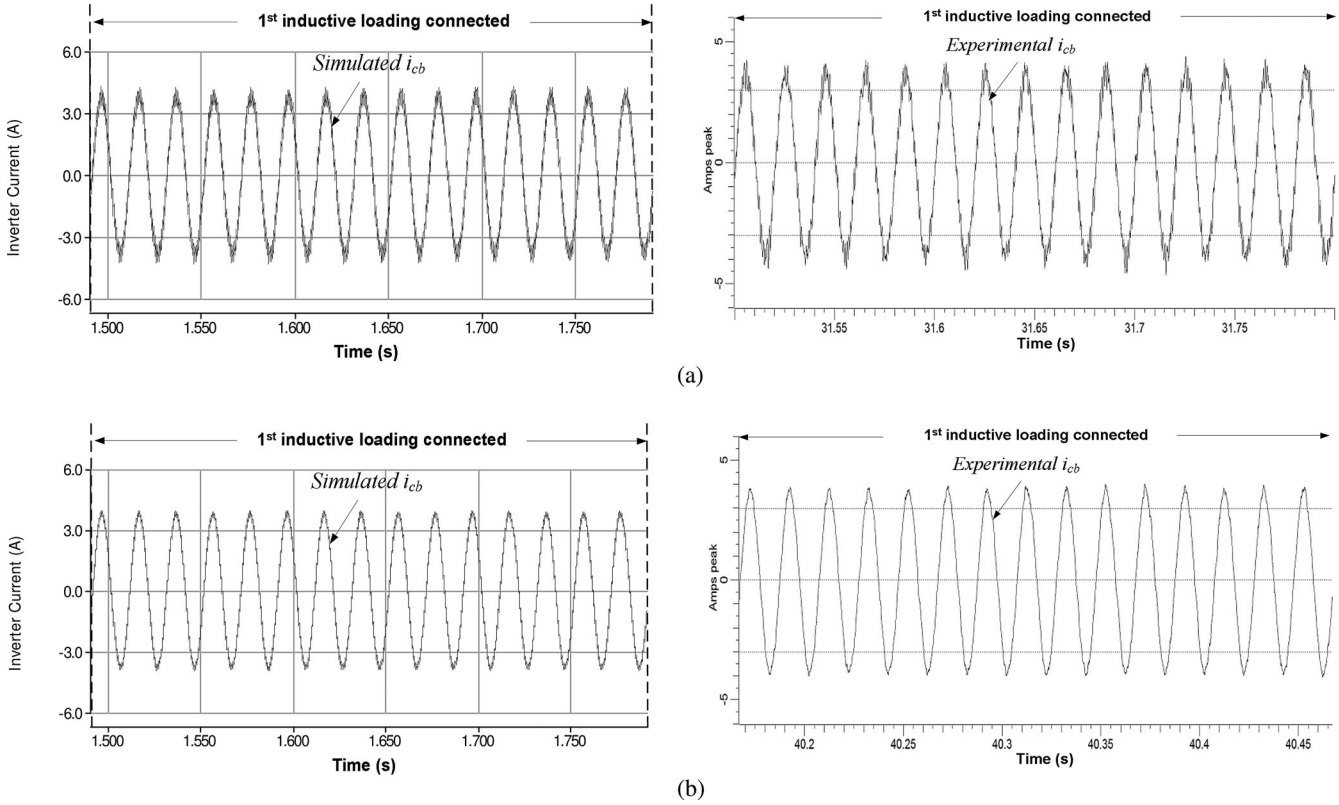

Fig. 13. Simulated and experimental i_{cx} of phase b with (a) a fixed V_{dc_U}, $V_{\mathrm{dc}_L} = 30$ V and (b) the proposed adaptive dc-link voltage control during undercompensation by passive part case.

traditional fixed dc-link voltage case. During overcompensation by passive part case, the similar simulated and experimental results can be obtained as well when both the first and second inductive loadings are connected.

From Figs. 6–14 and Tables IV–VII, verify that the proposed adaptive dc-link voltage-controlled *LC*-HAPF can obtain good dynamic reactive power compensation performance and reduce the system switching loss and switching noise.

In addition, the advantages offered by the proposed adaptive dc-link voltage control method for three-phase four-wire *LC*-HAPF system can also be achieved in a three-phase three-wire *LC*-HAPF system [12]–[14], [16]. With the help of the three-phase three-wire *LC*-HAPF modeling [16], the required minimum dc-link voltage $V_{\mathrm{dc\_min}\,x}$ with respect to different Q_{Lx_f} in (11) becomes

$$V_{\mathrm{dc\_min}\,x} = \frac{3\sqrt{2}}{2} V_x \left| 1 - \frac{Q_{Lx_f}}{\left| Q_{cx_{f\_PF}} \right|} \right|. \tag{13}$$

From Fig. 5, after replacing the determination of adaptive minimum dc-link voltage in the three-phase four-wire system part by a three-phase three-wire one as shown in Fig. 15, the proposed adaptive dc-link voltage control block diagram as shown in Fig. 5 can also be applied for the three-phase three-wire *LC*-HAPF.

Moreover, the proposed adaptive dc-link voltage control scheme for the *LC*-HAPF in this paper can also be extended to include current harmonics as well. When the current harmonics is also taken into consideration, from (11) and (13), there will be an extra harmonic component term added to the required minimum dc-link voltage $V_{\mathrm{dc\_min}\,x}$. Thus, the final three-phase required minimum dc-link voltage $V_{\mathrm{dc\_min}}$ for the *LC*-HAPF will be increased. Since this paper focuses on the adaptive dc-link voltage control for the three-phase four-wire *LC*-HAPF system in dynamic reactive power compensation, the adaptive dc voltage control details, simulation, and experimental results for the three-phase three-wire and three-phase four-wire *LC*-HAPF under fundamental reactive power and current harmonics consideration are not covered in this paper.

VI. Conclusion

An adaptive dc-link voltage-controlled *LC*-HAPF with dynamic reactive power compensation capability in the three-phase four-wire system is proposed in this paper. In order to implement the adaptive dc-link voltage control algorithm, the *LC*-HAPF required minimum dc-link voltage for compensating different reactive power is deduced and its adaptive control block diagram is also built. The final reference dc-link voltage is classified into certain levels for selection, so that the impact on the compensation performances by the fluctuation of the adaptive dc-link voltage in the practical case can be reduced. Moreover, the viability and effectiveness of the proposed adaptive dc-link voltage control for the three-phase four-wire *LC*-HAPF have been proved by both simulation and experimental results, in which it can achieve a good dynamic reactive power

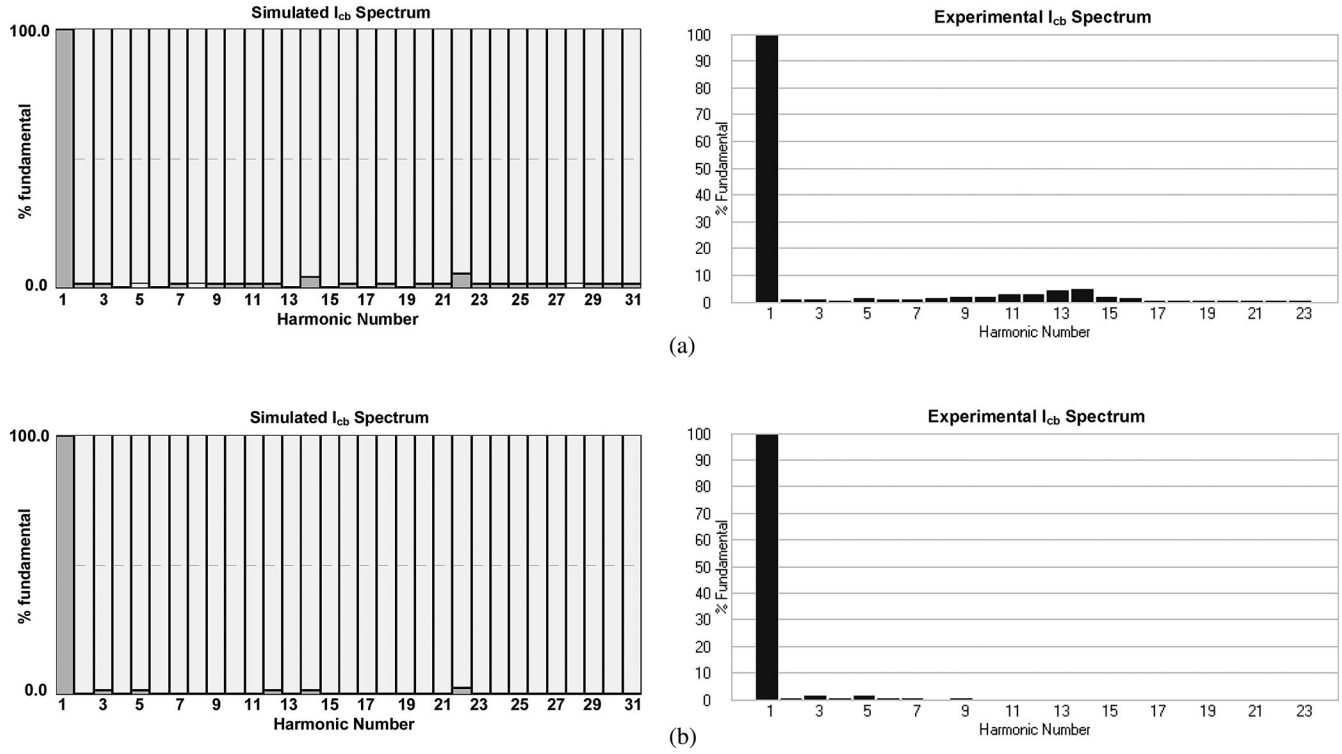

Fig. 14. Simulated and experimental frequency spectrum for i_{cx} of phase b with (a) a fixed V_{dc_U}, $V_{\mathrm{dc}_L} = 30$ V and (b) the proposed adaptive dc-link voltage control during undercompensation by passive part case.

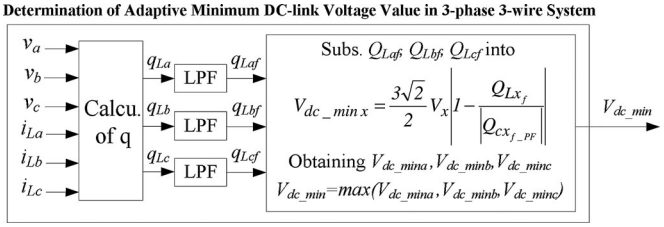

Fig. 15. Determination of adaptive minimum dc-link voltage in the three-phase three-wire system.

compensation performance as well as reducing the switching loss and switching noise compared with the traditional fixed dc-link voltage *LC*-HAPF. Therefore, the proposed adaptive dc-link voltage-controlled *LC*-HAPF is a cost-effective solution for dynamic reactive power compensation in practical situation. Nevertheless, this adaptive control method would not reduce the initial cost of the *LC*-HAPF because its maximum compensation range is merely determined by its specifications.

REFERENCES

[1] S. T. Senini and P. J. Wolfs, "Systematic identification and review of hybrid active filter topologies," in *Proc. IEEE 33rd Annu. Power Electron. Spec. Conf.*, 2002, vol. 1, pp. 394–399.

[2] P. Salmerón and S. P. Litrán, "A control strategy for hybrid power filter to compensate four-wires three-phase systems," *IEEE Trans. Power Electron.*, vol. 25, no. 7, pp. 1923–1931, Jul. 2010.

[3] A. Luo, W. Zhao, X. Deng, Z. J. Shen, and J.-C. Peng, "Dividing frequency control of hybrid active power filter with multi-injection branches using improved $i_p - i_q$ algorithm," *IEEE Trans. Power Electron.*, vol. 24, no. 10, pp. 2396–2405, Oct. 2009.

[4] A. Luo, Z. K. Shuai, Z. J. Shen, W. J. Zhu, and X. Y. Xu, "Design considerations for maintaining dc-side voltage of hybrid active power filter with injection circuit," *IEEE Trans. Power Electron.*, vol. 24, no. 1, pp. 75–84, Jan. 2009.

[5] A. Luo, C. Tang, Z. K. Shuai, W. Zhao, F. Rong, and K. Zhou, "A novel three-phase hybrid active power filter with a series resonance circuit tuned at the fundamental frequency," *IEEE Trans. Ind. Electron.*, vol. 56, no. 7, pp. 2431–2440, Jul. 2009.

[6] H. Fujita and H. Akagi, "Apractical approach to harmonic compensation in power systems: Series connection of passive and active filters," *IEEE Trans. Ind. Appl.*, vol. 27, no. 6, pp. 1020–1025, Nov./Dec. 1991.

[7] F. Z. Peng, H. Akagi, and A. Nabae, "A new approach to harmonic compensation in power systems: A combined system of shunt passive and series active filters," *IEEE Trans. Ind. Appl.*, vol. 26, no. 6, pp. 983–990, Nov./Dec. 1990.

[8] S. Park, J.-H. Sung, and K. Nam, "A new parallel hybrid filter configuration minimizing active filter size," in *Proc. IEEE 30th Annu. Power Electron. Spec. Conf.*, 1999, vol. 1, pp. 400–405.

[9] D. Rivas, L. Moran, J. W. Dixon, and J. R. Espinoza, "Improving passive filter compensation performance with active techniques," *IEEE Trans. Ind. Electron.*, vol. 50, no. 1, pp. 161–170, Feb. 2003.

[10] H. Fujita, T. Yamasaki, and H. Akagi, "A hybrid active filter for damping of harmonic resonance in industrial power systems," *IEEE Trans. Power Electron.*, vol. 15, no. 2, pp. 215–222, Mar. 2000.

[11] H. Akagi, "New trends in active filters for power conditioning," *IEEE Trans. Ind. Appl.*, vol. 32, no. 6, pp. 1312–1322, Nov./Dec. 1996.

[12] W. Tangtheerajaroonwong, T. Hatada, K. Wada, and H. Akagi, "Design and performance of a transformerless shunt hybrid filter integrated into a three-phase diode rectifier," *IEEE Trans. Power Electron.*, vol. 22, no. 5, pp. 1882–1889, Sep. 2007.

[13] R. Inzunza and H. Akagi, "A 6.6-kV transformerless shunt hybrid active filter for installation on a power distribution system," *IEEE Trans. Power Electron.*, vol. 20, no. 4, pp. 893–900, Jul. 2005.

[14] S. Srianthumrong and H. Akagi, "A medium-voltage transformerless ac/dc Power conversion system consisting of a diode rectifier and a shunt hybrid filter," *IEEE Trans. Ind. Appl.*, vol. 39, no. 3, pp. 874–882, May/Jun. 2003.

[15] H. -L. Jou, K. -D. Wu, J.- C. Wu, C. -H. Li, and M. -S. Huang, "Novel power converter topology for three phase four-wire hybrid power filter," *IET Power Electron.*, vol. 1, pp. 164–173, 2008.

[16] S. Rahmani, A. Hamadi, N. Mendalek, and K. Al-Haddad, "A new control technique for three-phase shunt hybrid power filter," *IEEE Trans. Ind. Electron*., vol. 56, no. 8, pp. 2904–2915, Aug. 2009.
[17] S.-U. Tai, M.-C. Wong, M.-C. Dong, and Y.-D. Han, "Some findings on harmonic measurement in Macao," in *Proc. 7th Int. Conf. Power Electron. Drive Syst*., 2007, pp. 405–410.
[18] M.-C. Wong, J. Tang, and Y.-D. Han, "Cylindrical coordinate control of three-dimensional PWM technique in three-phase four-wired trilevel inverter," *IEEE Trans. Power Electron*., vol. 18, no. 1, pp. 208–220, Jan. 2003.
[19] C.-S. Lam, M.-C. Wong, and Y.-D. Han, "Voltage swell and overvoltage compensation with unidirectional power flow controlled dynamic voltage restorer," *IEEE Trans. Power Del*., vol. 23, no. 4, pp. 2513–2521, Oct. 2008.
[20] H. Akagi, S. Ogasawara, and K. Hyosung, "The theory of instantaneous power in three-phase four-wire systems: A comprehensive approach," in *Conf. Rec. IEEE 34th IAS Annu. Meeting*, 1999, vol. 1, pp. 431–439.
[21] V. Khadkikar, A. Chandra, and B. N. Singh, "Generalized single-phase p-q theory for active power filtering: Simulation and DSP-based experimental investigation," *IET Power Electron*., vol. 2, no. 1, pp. 67–78, Jan. 2009.
[22] L. H. Wu, F. Zhuo, P. B. Zhang, H. Y. Li, and Z. A. Wang, "Study on the influence of supply-voltage fluctuation on shunt active power filter," *IEEE Trans. Power Del*., vol. 22, no. 3, pp. 1743–1749, Jul. 2007.
[23] M. Aredes, J. Hafner, and K. Heumann, "Three-phase four-wire shunt active filter control strategies," *IEEE Trans. Power Electron*., vol. 12, no. 2, pp. 311–318, Mar. 1997.
[24] N. Y. Dai, M. C. Wong, and Y. D. Han, "Three-dimensional space vector modulation with DC voltage variation control in a three-leg centre-split power quality compensator," *IEE Proc. Electr. Power Appl*., vol. 151, no. 2, pp. 198–204, Mar. 2004.

Chi-Seng Lam (S'04) received the B.Sc. and M.Sc. degrees in electrical and electronics engineering from the University of Macau (UM), Macao, China, in 2003 and 2006, respectively, where he is currently working toward the Ph.D. degree.

From September 2006 to June 2009, he was an E&M Engineer in the Campus Development and Engineering Section at UM. He has co-authored more than 20 technical journals and conference papers. His research interests include power electronics, power quality, and distribution flexible AC transmission system.

Mr. Lam received the 3rd Regional Inter-University Postgraduate Electrical and Electronic Engineering Conference Merit Paper Award in 2005.

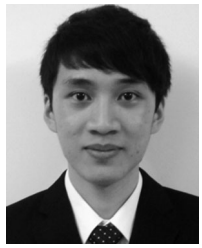

Wai-Hei Choi (S'09) received the B.Sc. degree in electrical and electronics engineering from the University of Macau (UM), Macao, China, in 2009, where he is currently working toward the M.Sc. degree.

He is with a Research Group of the Power Electronics Laboratory at UM. His research interests include power electronics, and energy-saving and power-quality compensators.

Mr. Choi received the Champion Award in the "Schneider Electric Energy Efficiency Cup," Hong Kong, 2010.

Man-Chung Wong (SM'06) received the B.Sc. and M.Sc degrees in electrical and electronics engineering from the University of Macau, Macau, China, in 1993 and 1997, respectively, and the Ph.D. degree from the Tsinghua University, Beijing, China, in 2003.

He has been an Associate Professor at the University of Macau since 2008. His research interests include flexible AC transmission system and distribution flexible AC transmission system, power quality, custom power, and pulsewidth modulation.

Dr. Wong received the Young Scientist Award from the "Instituto Internacional De Macau" in 2000, the Young Scholar Award from the University of Macau in 2001, and second prize of 2003 Tsinghua University Excellent Ph.D. Thesis Award.

Ying-Duo Han (SM'95) was born in Shenyang, Liaoning province, China, in 1938. He received the B.S. and M. S. degrees from the Department of Electrical Engineering, Tsinghua University, Beijing, China, in 1962 and 1965 respectively, and the Ph.D. degree in electrical engineering from Erlangen-Nuerenberg University, Erlangen, Germany, in 1986.

He is currently a Professor in the Department of Electrical Engineering, Tsinghua University, where he was the Vice-Chairman and Chairman from 1986 to 1995. Since 1989, he has been Head of Power Electronics Research Center, Tsinghua University. He is also a Visiting Professor at the University of Macau, China, and the Board Director of INESC-Macao.

Dr. Han received five Chinese State-level prizes, and seven first- and second-ranked Province-level and Ministry-level prizes. He is a Member of the Chinese Academy of Engineering.